This article has been accepted for publication in IEEE Access. This is the author's version which has not been fully edited and content may change prior to final publication. Citation information: DOI 10.1109/ACCESS.2026.3710444

IEEE Access
Multidisciplinary | Rapid Review | Open Access Journal

Date of publication xxxx 00, 0000, date of current version xxxx 00, 0000.

Digital Object Identifier

Towards Operational Use of the SOPHy X-Band Radar in Peru: A Bayesian Fuzzy Logic Approach for Ground Clutter Filtering in Complex Orography

CARLOS DEL-CASTILLO VELARDE[1], DANNY E. SCIPION[2], JAIRO M. VALDIVIA-PRADO[5], DANIEL MARTÍNEZ-CASTRO[1], YAMINA SILVA-VIDAL[1], RICARDO REINOSO-RONDINEL[3,4],

[1]Dirección de Ciencias de la Atmósfera, Hidrósfera y Cambio Climático, Instituto Geofísico del Perú (IGP), Lima, Perú
[2]Dirección de Ciencias del Geoespacio, Instituto Geofísico del Perú (IGP), Lima, Perú
[3]Civil Engineering, Hydraulics & Geotechnics, KU Leuven, Leuven, Belgium
[4]Royal Meteorological Institute of Belgium, Brussels, Belgium
[5]University of Colorado Boulder, Boulder, CO, USA

Corresponding author: Carlos Del-Castillo Velarde (e-mail: cdelcastillo@igp.gob.pe).

This work was supported by CONCYTEC under Contract PE501087421-2024 PROCIENCIA

ABSTRACT Ground clutter (GC) echoes can negatively impact the quality of radar measurements and derived products such as quantitative precipitation estimation. Therefore, effective removal of GC while preserving hydrometeor echoes is essential. The most advanced GC filtering techniques rely on polarimetric variables; however, radars without polarimetric capabilities are limited to spatial analysis of reflectivity, which reduces filtering performance. In this context, we propose a GC filtering algorithm based on fuzzy logic adapted to non-polarimetric variables for X-band radars. For demonstration, observations collected between January and March 2025 by an X-band radar located in the Mantaro Valley (Peru, 3300 m.a.s.l.) were analyzed. A representative dataset that included dry and rainy conditions was selected to derive the membership functions required for the fuzzy logic framework. Statistical results show that the bias in fractional area (dimensionless) caused by GC was reduced from 0.187 and 0.073 to -0.017 and -0.007 at elevation angles of 1.0° and 2.6°, respectively. Furthermore, the spatial analysis was performed separately in stratiform and convective precipitation. The stratiform case proved the most challenging due to the similarity in signal intensity and velocity with GC, leading to classification errors and loss of meteorological signal. These results show that the proposed method can be easily implemented using a small dataset in both dry and rainy conditions. We also demonstrate that GC can be successfully removed using only Doppler velocity and reflectivity measurements.

INDEX TERMS X-band radar, Ground Clutter, Fuzzy Logic, Complex Orography, Peru

I. INTRODUCTION

WEATHER radars provide detailed observations of the spatial and temporal structure of precipitating systems, providing essential inputs for monitoring rainfall, short-term forecasting, and hydrological modeling. Nevertheless, weather radar measurements are sensitive to a large number of error sources, for example, ground clutter echoes, beam-blockage, attenuation, and non-meteorological echoes. To achieve accurate radar-derived products, it is fundamental to apply a set of data quality control steps.

In particular, ground clutter (GC) is referred to as unwanted non-meteorological echoes resulting from, e.g., complex terrain, artificial structures, insects, and aircraft. Atmospheric conditions (air temperature, humidity, and pressure) also affect radar measurements, as they can modify beam propagation, leading to phenomena such as super-refraction, sub-refraction, or ducting (an extreme case of sub-refraction), and it is known as anomalous propagation [1]. it can affect the spatial distribution of echoes and can also increase the probability of observing GC, especially during convective storms where cold outflow winds favor its occurrence [2]. Dealing with this problem is not a simple task due to the spatiotemporal variability of atmospheric conditions and their limited sampled observations [3].

Currently, GC detection and filtering can be performed using two methodological approaches: spectral-level analysis and bulk moments level analysis (reflectivity, Doppler velocity, and spectrum width). At the Doppler spectrum level, techniques such as Gaussian model adaptive processing [4] have been developed for GC mitigation. However, this method can produce spectral leakage of GC echoes at velocities close to 0 m/s and, in its absence, may cause the loss of the meteorological signal [5], [6]. The CLEAN-AP methodology [7], implemented in the NEXRAD network, uses the autocorrelation spectral density, which preserves phase information, helping to identify intense narrow-band signals. When combined with adaptive windows, this approach reduces spectral leakage without increasing measurement uncertainty, outperforming the GMAP method. More recent methods propose filters based on image processing within the Doppler-range domain [5], as well as polynomial regression techniques to minimize errors associated with moving windows. These strategies allow for a more accurate capture of the low-frequency components characteristic of GC, thereby optimizing its detection and suppression [8]. At the bulk moments level, clutter identification techniques focus on the analysis of spatiotemporal characteristics. Various authors have proposed methods based on the variability of reflectivity. For example, [9] used the three-dimensional variability of reflectivity (fluctuations and vertical gradients) along with decision tree classification, while [10] introduced a texture analysis approach which, due to its simplicity, remains one of the most widely used methods. Similarity, [11] introduced a new metric known as the New Difference of Reflectivity (NDZ), which weights the vertical reflectivity gradient as a function of range.

Linked to GC echoes, statistical methods have made echo classification more appealing and flexible. [12] employed a Bayesian approach based on the height of the echo top and horizontal gradients, although they noted the need for local recalibration. [13] identified anomalous propagation under different precipitation regimes through spatial analysis of reflectivity (texture, gradients, fluctuations), fitting Gaussian distributions to construct a classification index. [14] used polarimetric and non-polarimetric variables together with Bayesian classification to define membership functions within a fuzzy logic technique. In addition, [15] demonstrated that the incorporation of polarimetric variables into Bayesian techniques significantly improves GC and anomalous propagation detection rates, reinforcing the advantages of polarimetric radars. Finally, with the rise of machine learning, techniques such as neural networks and the Chinese Restaurant Process have also been explored [16], [17], highlighting their superiority over classical techniques such as k-means.

The aforementioned studies were developed mainly for C- and S-band scanning radars. Although some of them have been adapted to X-band radars, which offer higher spatial resolution and sensitivity, these adaptations involve greater computational cost or require polarimetric variables [18]–[20]. Although polarimetric variables have been shown to be very useful for echo classification and radar data quality control, in some cases, this technology is not available due to technical problems, poor data quality, or because the systems have been decommissioned [21]–[23].

Despite advances in dual-polarization radar observations and listed error sources, the most widely used radar measurement for QPE applications remains reflectivity, even when compared with differential phase-based techniques, which are not straightforward to implement [24]. Rainfall rates are typically derived from radar measurement through regionally dependent statistical relationships. However, a quality control process is essential to ensure accurate estimates. In this context, it is necessary to develop a processing algorithm that is independent of polarimetric variables and that can be easily adapted to the various radar bands. Consequently, this study proposes a fuzzy logic-based framework for GC filtering. Unlike previous works that have implemented similar methodologies, this study emphasizes the use of non-polarimetric radar variables for the design of membership functions following a Bayesian approach. In contrast to predefined membership functions (e.g. trapezoidal or triangular), the proposed approach captures the statistical variability of radar measurements and adapts the GC filter to the specific characteristics of the radar and local environmental conditions. We found that our method generally performs better in the complex topography of Peru than other methods, such as the Gabella filter, which is widely used for GC filtering in single-polarization radar systems. This improvement is particularly evident at the lowest elevation angle (1.0°), where the Gabella filter shows limited capability to remove GC echoes under dry conditions.

The article is organized as follows: Section 2 describes the topographic characteristics of the study area and the cases used for validation. Section 3 presents in detail the construction of the clutter mask and the methodological framework used to evaluate its performance. Section 4 analyzes the case studies, the overall performance of the method over several months, and provides a comparison with the widely applied Gabella filter. Finally, we summarize our main results in the conclusions section.

II. RADAR DATA AND STUDY AREA

A. THE SOPHY RADAR

The Scanning-system for Observation of Peruvian Hydrometeorological (**SOPHy**) is a dual-polarization weather radar operating at a frequency of 9.345 GHz (X-band) [25], [26]. SOPHy has collected data since December 2022 and is capable of scanning an area of up to 60 km in approximately 70 s with a range resolution of 60 m. The SOPHy radar has two operating modes known as Range Height Indicator(RHI) and Plan Position Indicator (PPI), and records variables such as reflectivity (Z), radial velocity (V), spectrum width (W),

TABLE 1. Technical Parameters of the SOPHy Radar [25]

Parameter	Value
Frequency	9.345 GHz
Maximum Range	60 km
Range resolution	60 m
Polarization	Dual polarization
Max Angular Speed	20° s^{-1}
Modes	PPI and RHI
Beam Width	1.8°
Antenna diameter	1.21 m
Antenna Gain	38.5 dBi

differential reflectivity (Z_{dr}), differential phase (ϕ_{dp}), and correlation coefficient (ρ_{hv}). However, due to technical issues affecting its second Tx/Rx channel, the quality of the polarimetric data deteriorated. Since 2024, the system has been operating with only a single channel, and therefore only Z, V and W measurements are currently available. A summary of the technical specifications of the SOPHy radar is shown in Table 1.

In January 2025, SOPHy was installed at ground level at the Sicaya Observatory of the Geophysical Institute of Perú (IGP), located in the province of Huancayo (12° 02' 24" S, 75° 17' 46" W; Fig. 1). It is configured to perform a scanning pattern that includes five PPIs at elevations of 1.0°, 2.6°, 4.2°, 8.0°, and 12.0°, and one RHI at an azimuth of 350.0°. The data are stored in HDF5 format and compressed as `.tar.gz` files, where each compressed file contains all recorded variables for a given elevation angle. The dataset is available at the following link: https://www.igp.gob.pe/observatorios/radio-observatorio-jicamarca/database/dataset/?voc_station_name=Huancayo

B. STUDY AREA

The Mantaro river basin is situated in the central Peruvian Andes, specifically in the department of Junín, and it is located between latitudes 10° 33' 52.66" - 13° 32' 31.39" and longitudes 73° 55' 10.88" - 76° 39' 16.01" (Fig. 1), with a total area of 34 546.51 km^2. In the central part of the basin lies the Mantaro Valley, with an average altitude of 3 300 m above sea level. Its precipitation regime occurs mainly between October and April, with monthly totals ranging between 60 mm and 130 mm [27], and the accumulated rainfall during these months represents 83% of the annual precipitation [28]. Since the Mantaro Valley is surrounded by the Andes, it presents complex topography that plays an important role in the local climate and in precipitation formation.

To determine the impact of the surrounding topography of the Andes on SOPHy radar's scans, the beam blockage fraction (BBF) was estimated using the wradlib library [29] and Digital Elevation Model at various elevation angles, considering the radar location and beam geometry. Fig. 2 shows the resulting beam blockage fields where BBF equal to 1 indicates a fully beam blockage. It can be seen that, at the lowest elevation of 1.0°, a significant extent of the radar's range is obstructed, limiting clear observations to a 10 km

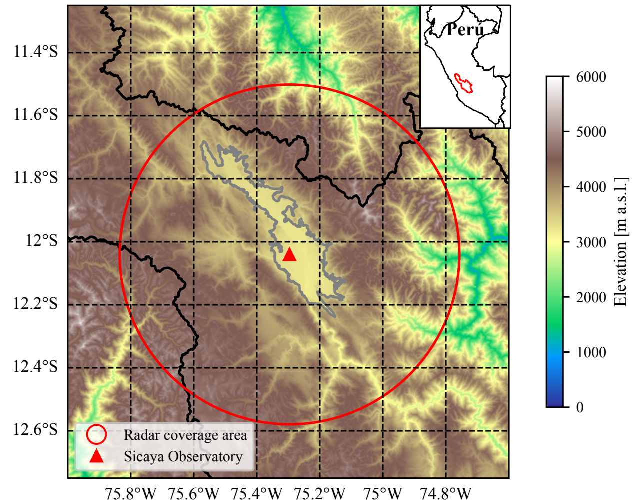

FIGURE 1. Digital Elevation Model (Shuttle Radar Topographic Mission) of the Mantaro valley. The solid black line is the boundary of the Mantaro River basin and the solid gray line is Mantaro Valley. The red triangle indicates the SOPHy location, and the red circle represents its range of 60 km

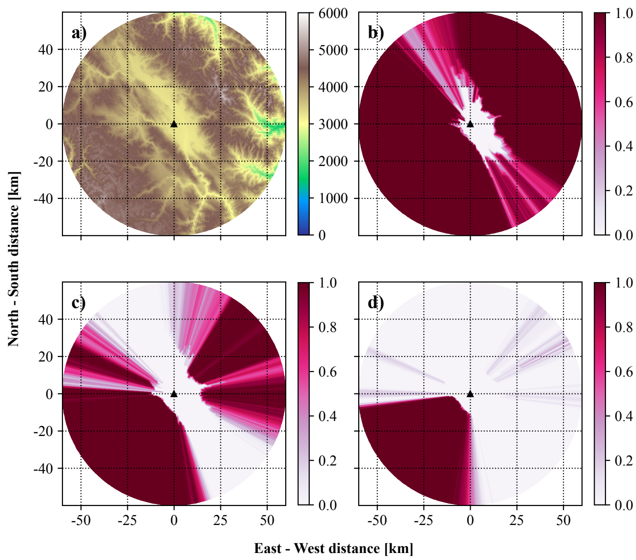

FIGURE 2. SOPHy's beam blockage fraction caused by topography. DEM of the Mantaro valley (a) and BBF maps at elevation angles of 1° (b), 2.6° (c), and 4.2° (d)

radius. However, at elevations of 2.6° and 4.2°, the beam successfully propagates along the Mantaro Valley axis and toward the eastern flank of the cordillera . Above 8°, the topography no longer interferes with the beam propagation, allowing free-blockage scans (not shown).

C. DATASET

The dataset used in this study covers the period from January to March 2025 and includes a total of 11 643 volumetric scans. During this period, two datasets were selected corresponding to clear-sky conditions (dry conditions) and precip-

TABLE 2. Fuzzy Logic Dataset 2025

Dataset	Elevations	Days	N° PPI
Clear-sky	1° and 2.6°	January 26	132
		January 30	221
Precipitation	8° and 12°	March 13	116
		March 14	101
		March 18	68
		March 20	74
		March 22	84
		March 23	58
		March 30	93
		March 31	84

itation conditions which include different types of rain (Table 2). These datasets were used to determine the membership functions required for the fuzzy logic approach (III-A).

In the clear-sky dataset, only elevations with significant GC echoes (1.0° and 2.6°) were considered, as these were previously identified through visual inspection of the radar data. In contrast, under precipitation conditions, the 8° and 12° elevations were selected to ensure the absence of GC echoes. Since the purpose of the fuzzy logic algorithm is to separate GC and meteorological echoes, both liquid and solid precipitation were included.

In addition, four representative cases were selected from the dataset shown in Table 2 to assess the algorithmś capability to separate precipitation and GC in scenarios where both signals are either spatially isolated or overlapping. Case 1 (January 30) represents clear-sky conditions. Case 2 (March 13) corresponds to convective precipitation, where the system partially extends over the region affected by GC. Case 3 (March 14) involves widespread stratiform precipitation. Finally, Case 4 (March 18) includes convective precipitation in a region free of GC.

For validation purposes, we used 2 873 volumetric scans collected between February 1 and March 31, 2025, a period characterized by a higher frequency of precipitation events. Only complete scans, defined as those containing all elevation angles, were included in the analysis. Additionally, data from March 26, 28, and 29, 2025 were excluded due to anomalous measurements.

III. METHODOLOGY

A. FUZZY LOGIC METHODOLOGY

The core of the fuzzy logic methodology is the determination of the membership functions (*mf*), which are responsible for assigning or quantifying the degree of membership of each numerical input or field to a specific class. This process is known as fuzzification. The *mf* can be derived from an initial dataset referred to as training data, either in combination with conditional probability [30] or through the use of a Bayesian classifier [14], [30]–[32]. The membership function can be expressed as follows:

$$mf(X) = P(C|X) = \frac{P(X|C)P(C)}{P(X)} \tag{1}$$

where

- X denotes the input field to be evaluated;
- $P(C)$ is the probability distribution function of clutter;
- $P(X)$ is the probability distribution function of the input field;
- $P(X|C)$ represents the conditional probability under clutter conditions.

Assuming that only two types of echoes are considered in the classification (GC and precipitation), and applying the law of total probability, (1) can be rewritten as (2) to express *mf* as a function of the clutter ($P(C)$) and precipitation ($P(R)$) distributions, as well as the corresponding conditional probabilities ($P(X|C)$ and $P(X|R)$). Since the prior probabilities $P(C)$ and $P(R)$ are unknown, both are assumed to be equally probable ($P(C)$=$P(R)$=0.5), as proposed by [33]. Therefore, (2) simplifies to (3):

$$mf(X) = \frac{P(X|C)P(C)}{P(X|C)P(C) + P(X|R)P(R)} \tag{2}$$

$$mf(X) = \frac{P(X|C)}{P(X|C) + P(X|R)} \tag{3}$$

Previous studies based on fuzzy logic [2], [34], [35] have identified various inputs fields (X) useful for detecting GC or anomalous propagation. In particular, texture, fluctuations along the radial axis (SPIN), and vertical gradients are primarily associated with Z, while standard deviation or mean values are related to V, W, and polarimetric variables. The membership degree is determined by evaluating the input field in its corresponding membership function, which assigns a value between 0 and 1, where each input field is associated with its own membership function. The resulting membership degrees represent partial conditions and are combined using fuzzy logical operators ('OR' or 'AND') to obtain a joint membership degree, which is used to determine the final clutter probability. According to [14], the 'AND' operator can be represented by the product or minimum of all membership degrees, while the 'OR' operator can be represented by weighted sum or maximum. Finally, a threshold is applied to the clutter probability to determine the final classification, where values above the threshold are classified as clutter and values below it as precipitation; a threshold of 0.5 is commonly used.

B. SOPHY GC FILTER DESIGN

The clutter mask generation process can be summarized in five main steps: 1) membership function design; 2) fields calculation; 3) transformation of fields into membership degrees; 4) combination of membership degrees; and 5) clutter mask estimation. The sequence of steps is shown in (Fig. 3).

This article has been accepted for publication in IEEE Access. This is the author's version which has not been fully edited and content may change prior to final publication. Citation information: DOI 10.1109/ACCESS.2026.3710444

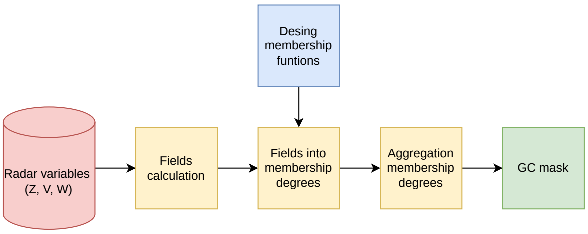

FIGURE 3. **Schematic of the fuzzy logic algorithm. The input variables are *Z*, *V* and *W* in polar coordinates, and the output is a binary clutter mask.**

TABLE 3. **Fields Used for Clutter Detection**

Variable	Field	Abbreviation	Window Size
Radial Velocity	Median	MDVE	5x5
Radial Velocity	Circular STD	SDVE	5x5
Spectrum Width	Median	MDSW	5x5
Reflectivity	Texture	TDBZ	3x3
Reflectivity	Spin	SPIN	5x9

The design of the membership functions is performed only once. For this purpose, and for each selected input X,(3) is adopted as the starting point, where $P(X|C)$ and $P(X|R)$ are derived from dry and precipitation conditions, respectively, as shown in Table 2, using the probability distribution function of X

In our case, X is given by five fields, prioritizing the use of non-polarimetric variables; these were calculated over windows of size $n \times m$ from the fields shown in Table 3.

The circular standard deviation (σ_c) [36] was employed instead of the classical standard deviation due to the periodical nature of Doppler velocity when the Nyquist velocity is exceeded, known as aliasing. In this context, σ_c accounts for angular dispersion and is therefore unaffected by aliasing [37], allowing for better discrimination between meteorological and non-meteorological echoes. The circular standard deviation is defined as:

$$\sigma_c = \sqrt{-2\ln\left|\frac{1}{N}\sum_{k=1}^{N} e^{j\theta_k}\right|} \tag{4}$$

where $\theta = \pi V/V_{nyq}$ is the angle in radians, V is the Doppler velocity, V_{nyq} is the Nyquist velocity, N is the window size and $\ln$ denotes the natural logarithm.

Reflectivity texture is defined by (5) [35] and quantifies the spatial variability relative to the central pixel value within a 3×3 window. Therefore, lower values indicate a uniform reflectivity field, whereas higher values highlight the irregular and discontinuous nature typical of ground clutter. The TDBZ field is calculated as

$$\mathrm{TDBZ}(Z_{a,b}) = \frac{\sum_{i=-(m-1)/2}^{+(m-1)/2}\sum_{j=-(n-1)/2}^{+(n-1)/2}\left(Z_{a,b} - Z_{a+i,b+j}\right)^2}{m\,n} \tag{5}$$

where m and n denote the window size, a and b denote the indices of the central pixel of the window, and Z denotes reflectivity (dBZ).

Finally, SPIN is defined as the number of reflectivity changes exceeding 2 dBZ along the radial direction within an 11 (azimuth) $\times$ 21 (range) window [9], expressed in percentage terms. According to [9], while the algorithm performs adequately with WSR-88D data, it may require fine-tuning when applied to other radars or different scanning strategies. In the present study, the window size was reduced to 5×9 to adapt it to the spatial resolution of the SOPHy radar.

Although the vertical reflectivity gradient has proven to be an effective indicator of GC, it was excluded from this study because GC contamination is present across the first three elevation levels. This overlap complicates identification, especially during convective events with significant vertical development. Fig. 4 shows the membership functions estimated for the SOPHy radar. It can be observed that the GC probability function (blue line) for the reflectivity-related fields (Fig. 4d and 4e) maintains an upward trend, resulting in high spatial variability of GC. Furthermore, the TDBZ and SPIN fields show a clear separation between meteorological and non-meteorological echoes.

Regarding the fields associated with radial velocity, SDVE (Fig. 4b) exhibits a rapidly decreasing probability function. This behavior is a consequence of the low angular dispersion of Doppler velocities in non-meteorological echoes. Meanwhile, MDVE shows a probability function where GC probability increases sharply around 0 m/s, due to the stationary nature of GC echoes. Lastly, spectrum width (Fig. 4c) exhibits a bimodal probability function centered around 0 and 1 m/s, respectively, indicating its limited skill in discriminating GC echoes.

For each PPI at the elevations angles shown in 2, the five previously mentioned input fields are calculated. Then, each field is evaluated using its corresponding membership function to obtain the partial clutter probabilities (membership degrees) of each field. Among the fuzzy-logical operators used to combine the partial probabilities, the weighted sum was selected because it allows flexible weighting of each field according to its relative importance. In this study, a detailed optimization of the field weights was not performed. Instead, the weights were assigned based on the behavior observed in the membership functions. Accordingly, weights of 0.35, 0.20, 0.05, 0.20, and 0.20 were assigned to MDVE, SDVE, MDSW, TDBZ, and SPIN, respectively. Finally, a threshold value of 0.5 is applied to the resulting aggregated clutter probability to generate a binary clutter classification mask.

As an additional and independent step from the fuzzy logic process, morphological operators [38] were applied to refine the GC mask. Opening and closing operations with a disk-shaped structuring element of one-pixel radius were used to remove small artifacts and reconnect isolated pixels. These operations help delineate contaminated areas and reduce classification errors, particularly in situations where the wind direction is perpendicular to the radar beam, producing

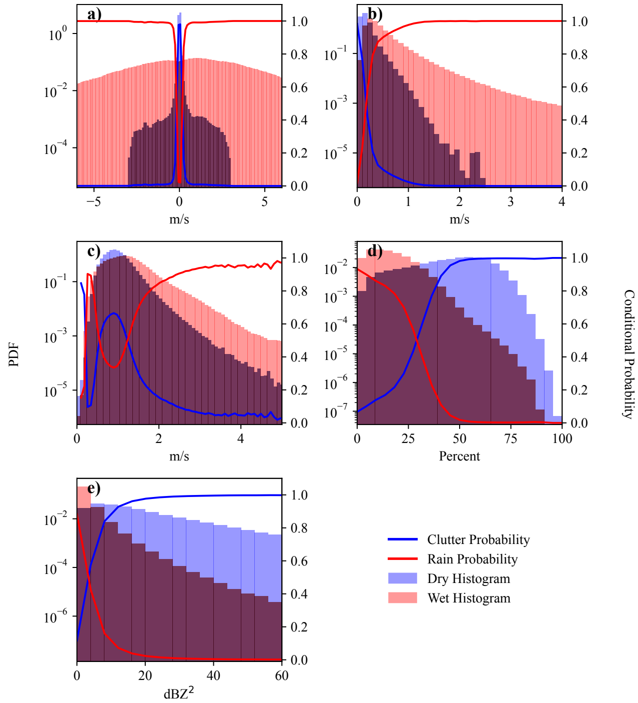

FIGURE 4. Probability distribution function (left y-axis) and Membership functions (right y-axis) determined for the SOPHy radar for: (a) MDVE, (b) SDVE, (c) MDSW, (d) SPIN, and (e) TDBZ

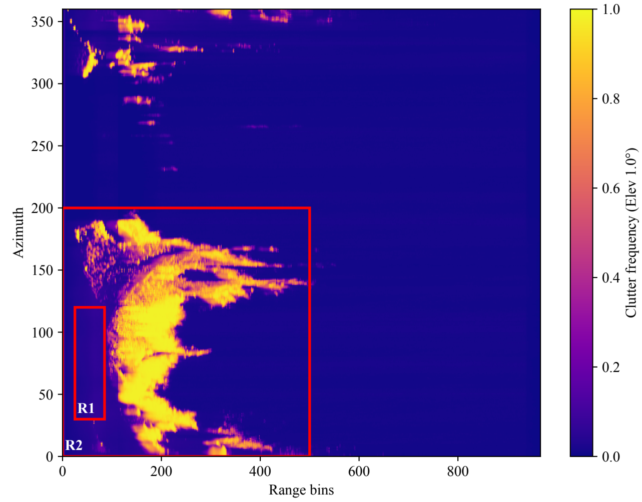

FIGURE 5. Frequency map of GC occurrence at a 1.0° elevation, estimated from volumetric scans collected between January and March 2025. The map was computed as the occurrence frequency of echoes at each range gate (x-axis) and azimuth bin (y-axis), normalized by the total number of samples. R1 denotes the GC-free region, while R2 identifies the area selected for algorithm evaluation.

apparent radial velocities close to zero.

C. VALIDATION APPROACH

Performance evaluation of classification algorithms commonly relies on metrics such as the Probability of Detection (POD) and False Alarm Ratio (FAR). However, these metrics require a static ground truth to quantify classification performance. Ideally, GC should remain constant over time; nevertheless, in practice, it exhibits small variations. Furthermore, in cases where precipitation echoes are more intense than GC echoes, these variations can become even more pronounced. Due to these temporal fluctuations in GC, establishing a reliable reference to accurately apply metrics like POD or FAR is challenging. In this work, a linear model is proposed to explain the composition of meteorological and GC echoes at each time step. This linear model is defined by Equation (6):

$$A_{total} = \beta A_{meteo} + A_{clutter} + \epsilon \tag{6}$$

where A_{total} denotes the total detected echo area, A_{meteo} represents the meteorological contribution, $A_{clutter}$ represents GC contamination, β is a weighting factor that quantifies the relative contribution of meteorological echoes, and ϵ is a residual term. If $\beta \approx 0$, the system is dominated by GC, whereas if $\beta \approx 1$, meteorological echoes become the dominant contribution.

In this framework, all area terms are defined as the ratio between the number of valid pixels (non-missing data) and the total number of pixels within the analysis domain (area fraction), with A_{meteo} corresponding to observations at the 8.0° elevation angle.

Equation (6) is evaluated in region R2 (Fig. 5), which is characterized by a strong presence of GC and a high frequency of precipitation events. This evaluation is performed both before and after applying the GC filtering, and the performance is measured based on the algorithm's ability to reduce the Root Mean Squared Error (RMSE) and BIAS, as well as to increase the correlation between A_{total} and A_{meteo}. Additionally, FAR metric is included but restricted to region R1 (Fig. 5), where no GC echoes are present. In this manner, the failure probability of the proposed algorithm is correctly quantified

IV. RESULTS AND DISCUSSION

A. DIURNAL VARIATIONS IN GC

During the clear-sky days (January 26 and 30), the factor β is zero, and therefore $A_{total} = A_{clutter} + \epsilon$. Fig. 6a shows A_{total} at R2 for the 1.0°, 2.6°, and 4.2° elevation angles, where $A_{clutter}$ represents the mean GC area and ϵ represents its temporal variability. At the lowest elevation angle, the mean area was 0.206, with values ranging from 0.172 to 0.255. At the highest elevation angle, the mean area was 0.018, with values ranging from 0.014 to 0.028.

At the 1.0° elevation, which exhibits the highest varibility, the minimum GC area was observed between 07:00 and 08:00 UTC-5, coinciding with the minimum temperature. Conversely, peak areas occurred during the afternoon (15:00-17:00 UTC-5), when maximum temperatures were reached. Similar results were reported by [12]. These variations could be associated with anomalous propagation of the radar beam, driven by changes in the atmospheric refractive index, or

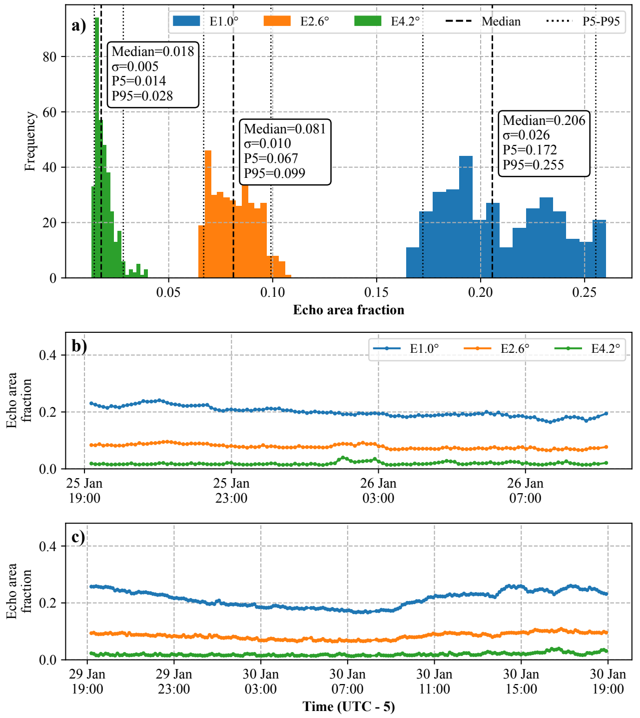

FIGURE 6. Temporal variability and characterization of the area fraction under dry conditions. (a) Frequency distribution for three elevations (1.0°, 2.6°, and 4.2°), (b) temporal variability of 26/01/2025 and (c) temporal variability of 30/01/2025

with antenna sidelobes. The latter explains the high variability observed at the lowest elevation angles.

B. CASE ANALYSIS

Fig. 7 and Fig. 8 display the four representative cases (section II-C) before and after applying the GC filter, respectively. GC echoes are primarily distributed along the eastern flank of the radar and persist up to the 4.2° elevation, with values ranging between 20 dBZ $< Z <$ 40 dBZ (Fig. 7, a-d). It is clearly observed that in Case 1, the GC filter removes the totality of contaminated pixels, demonstrating its efficacy under dry conditions (Fig. 8, a-d). Convective events (Cases 2 and 4) are characterized by reflectivity values $Z > 42$ dBZ and strong Doppler velocity gradients, which facilitate the correct classification of GC echoes, as the latter are typically less intense ($Z < 40$ dBZ) and stationary. These distinct physical signatures help preserve meteorological echoes at low elevations while simultaneously maintaining the vertical structure of the cloud.

In contrast, the stratiform event (Case 3) is characterized by Z values $<$ 40 dBZ and weak, homogeneous Doppler velocity gradients. Since these features are similar to those of GC, preserving meteorological echoes becomes more difficult, increasing classification errors. Due to the heavy presence of GC at 1.0° and 2.6° elevations, the vertical structure of the cloud is not adequately preserved in this case.

The temporal variability of both meteorological and non-meteorological echo area fractions for the four aforementioned cases is shown in Fig. 9. In Case 1, the fraction areas exhibit a clear separation between the 1.0°, 2.6°, 4.2°, and 8.0° elevations (Fig. 9a), which is proportional to the amount of GC echoes present. After removing the contaminated pixels, the areas decrease to values near zero, evidencing the filter's efficacy under dry conditions. A similar behavior is observed in Case 4, where GC and meteorological echoes do not overlap; this allows for the removal of contaminated pixels without compromising the meteorological signal. This is reflected in the post-filtered areas, which become similar and consistent across the different elevations.

Unlike Cases 1 and 4, Cases 2 and 3 do not exhibit area stratification due to the overlapping of GC and meteorological echoes. After removing the contaminated pixels, it was observed that not all meteorological echoes could be recovered at the 1.0° and 2.6° elevations, resulting in smaller areas compared to the higher elevations as a consequence of overfiltering. Nevertheless, it is important to highlight that in the convective precipitation event (Case 2), the high reflectivity values allowed for a greater recovery of the meteorological area at the lowest elevation compared to the stratiform precipitation event (Case 3).

Additionally, FAR time series was estimated for the precipitation cases 2, 3, and 4. In Cases 2 and 4, the FAR calculated for region R1 (Fig. 10) is below 3%, whereas for stratiform precipitation (case 3), it exceeds 3% and can reach values above 10%. The increase in false positives during the stratiform event is primarily attributed to low-intensity or near-zero Doppler velocities, which occur frequently in this type of precipitation. These are associated with the cloud dissipation phase during the last 10 min of case 3 and the zero isodop phenomenon [13], which can extend over several kilometers.

C. STATISTICAL PERFORMANCE

To evaluate the overall performance of the proposed algorithm, the linear model described in III-C was applied to 2 873 volumetric scans collected between February 1 and March 31, 2025. This analysis aims to assess the algorithm's ability to reduce bias/intercept and to quantify the degree of correlation between A_{total} and A_{meteo} after applying the GC filter. The results of this analysis are summarized in Table 4.

Fig. 11 shows the linear model before applying the GC filter. The results indicate intercept values of 0.215, 0.081, and 0.021 for the 1.0°, 2.6°, and 4.2° elevations, respectively. Note these values are similar to the mean GC fraction areas estimated under dry conditions (Fig. 6a), indicating that the linear model adequately represents the area contaminated by GC. Additionally, the residual analysis shows that the interval between the 5th and 95th percentiles (P5-P95) is also consistent with the one observed under dry conditions, suggesting that the model also accurately reproduces the diurnal variability of the GC.

After applying the fuzzy GC filter (Fig. 12), the model intercept was reduced to approximately 0 across all elevations. Likewise, the RMSE decreased from 0.199, 0.078, and 0.034 to 0.024, 0.017, and 0.020 for the 1.0°, 2.6°, and

This article has been accepted for publication in IEEE Access. This is the author's version which has not been fully edited and content may change prior to final publication. Citation information: DOI 10.1109/ACCESS.2026.3710444

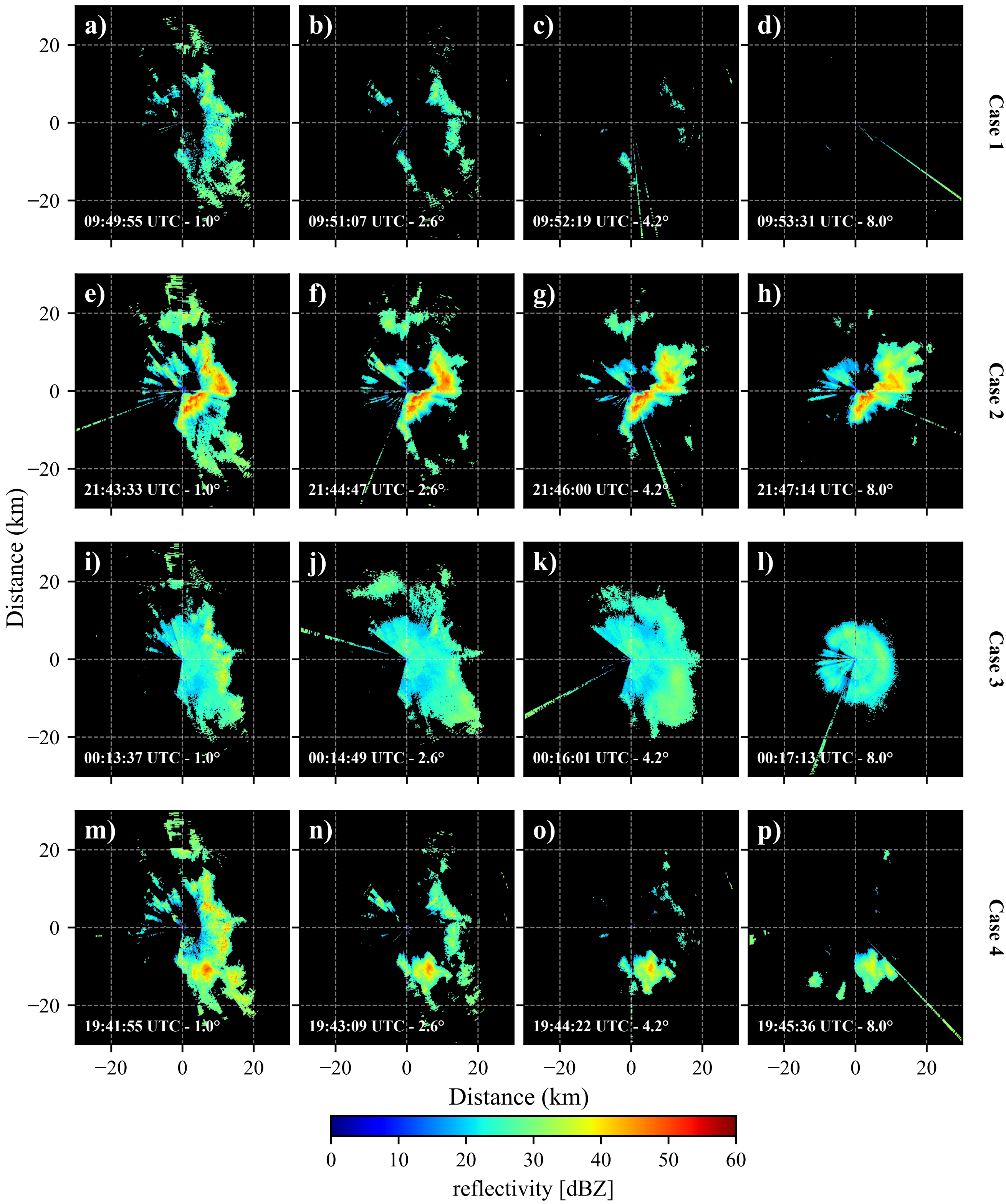

FIGURE 7. Reflectivity PPI panels without GC filtering at four elevation angles (1.0°, 2.6°, 4.2°, and 8.0°) for four study cases. Case 1: No rain; Case 2: Widespread convective precipitation; Case 3: Stratiform precipitation; and Case 4: Localized convective precipitation.

4.2° elevations, respectively. These results indicate that the proposed filter effectively removes both GC and anomalous

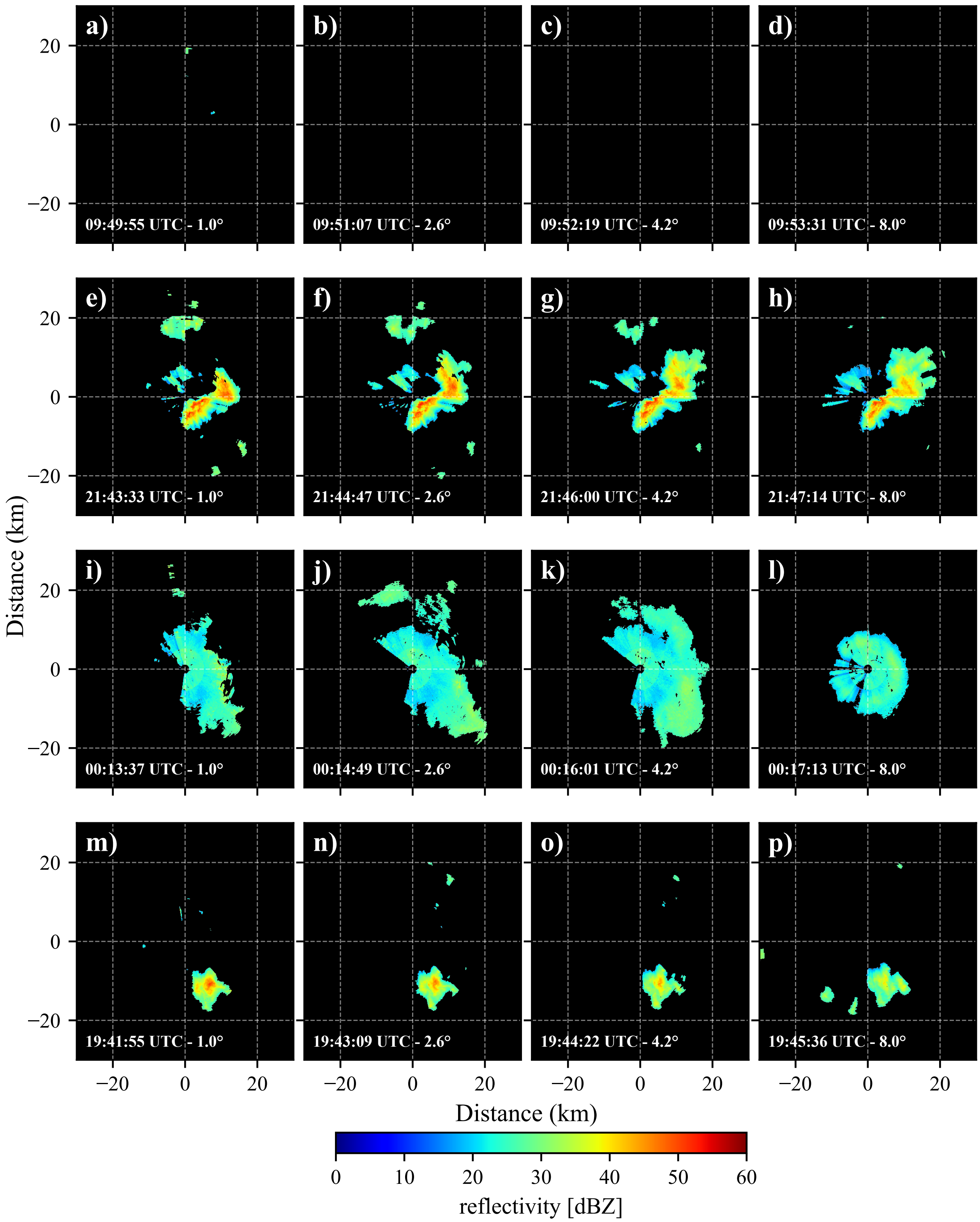

FIGURE 8. Same as Figure 7, but after applying the GC filter

propagation effects. The negative bias observed at the 1.0° and 2.6° elevations is attributed to over-filtering, due to the vast extent of contaminated echoes present at these angles. Conversely, the positive bias at the 4.2° elevation is primarily

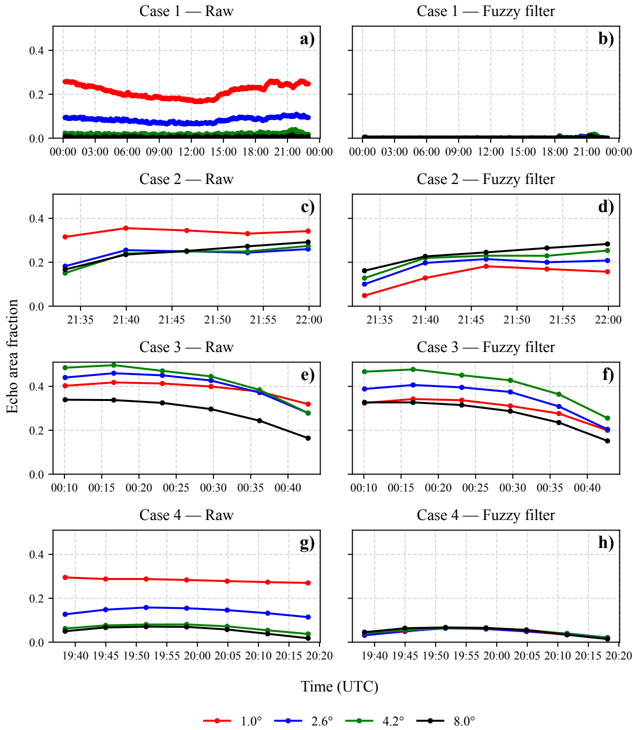

FIGURE 9. Comparison of the echo area time series before (left column) and after GC filtering (right column). Four events in 2025 are analyzed across different elevation angles (1.0° to 8.0°).

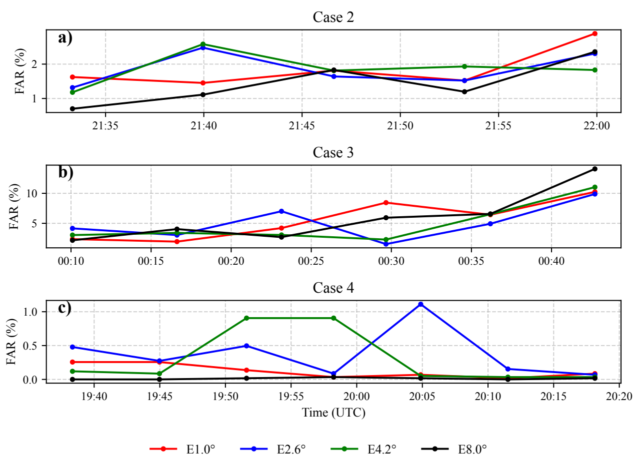

FIGURE 10. Same as Figure 9, but for FAR.

TABLE 4. Statistical Comparison Between Raw and Fuzzy Filter Echo Area Fraction

Elevation	Raw			Fuzzy filter		
	1.0°	2.6°	4.2°	1.0°	2.6°	4.2°
Intercept	0.215	0.081	0.021	0.006	0.003	0.001
RMSE	0.193	0.077	0.039	0.027	0.021	0.025
Bias	0.187	0.073	0.028	-0.017	-0.007	0.005
R^2	0.38	0.83	0.88	0.88	0.89	0.88

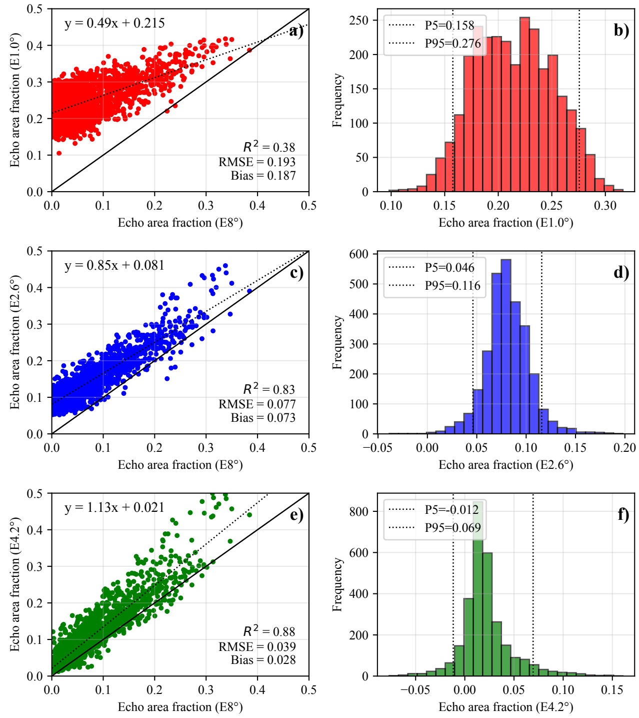

FIGURE 11. Linear regression analysis and residual distributions of raw echo area fractions between January and March 2025. Panels (a), (c), and (e) show the linear regression fit (dashed line) together with the 1:1 identity line (solid line) for elevations E1.0°, E2.6°, and E4.2°, respectively. Panels (b), (d), and (f) present the corresponding residual distributions, including the P5 and P95 percentiles (dotted lines).

associated with larger stratiform precipitation areas than those observed at the 8° elevation (Fig. 12e). Due to the beam geometry and the limited vertical development of this type of precipitation, the area at this elevation is larger than the reference area at 8.0° (Fig. 7k,l), which explains the resulting bias. Furthermore, the correlation improves once GC is removed, indicating that the vertical structure of the echoes is consistent across different elevations.

Note that the residuals after removing the GC are centered around 0 (Fig. 12). While these small variations are relative to the reference area (8.0°), they can also be interpreted as natural vertical changes in the cloud structure.

D. COMPARISON WITH GABELLA FILTER

One of the filters commonly used for the removal of GC echoes, due to its simplicity, is the Gabella filter [10]. This filter is based on the analysis of reflectivity texture to identify areas contaminated by GC. An important aspect to consider is that the Gabella filter assumes that GC echoes exhibit higher intensities than meteorological echoes [39]. However, as shown in Fig. 7, GC echoes are not always more intense than meteorological echoes. Fig. 13 shows a comparison between fuzzy logic-based filtering approach and the Gabella filter for the four case studies previously analyzed. It is observed that the Gabella filter is not capable of completely removing GC echoes, which is particularly evident in the absence of precipitation (Case 1), where contaminated areas persist at

This article has been accepted for publication in IEEE Access. This is the author's version which has not been fully edited and
content may change prior to final publication. Citation information: DOI 10.1109/ACCESS.2026.3710444

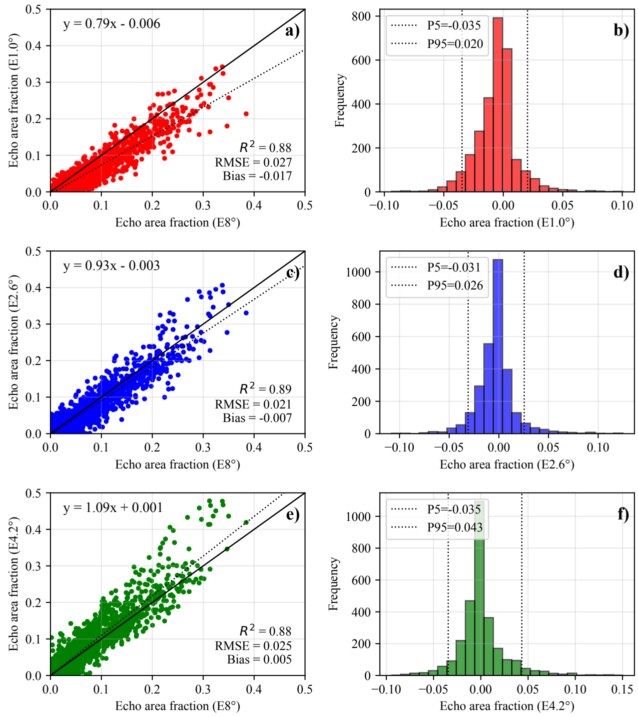

FIGURE 12. Same as Figure 11, but after applying fuzzy filter

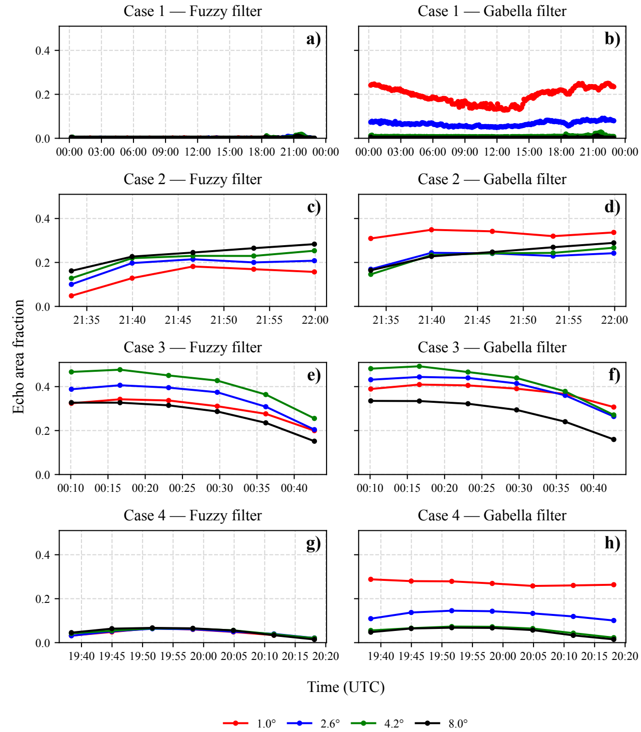

FIGURE 13. Comparison of the time series of the echo area fraction processed using fuzzy logic and the Gabella algorithm.

the 1.0° and 2.6° elevations. The limited performance of the Gabella filter at low elevations (1.0° and 2.6°) indicates that this method is not able to adequately handle extensive areas contaminated by GC, whereas its effectiveness increases when the affected regions are smaller in extent. In this regard, [40] recommend that texture-based algorithms be used as a post-processing stage, after a prior GC filtering method has already been applied.

V. CONCLUSION

This work presents a fuzzy logic GC echo filter that is designed for the SOPHY X-band in complex geography and without the usage of dual-polarization bulk moments. The advantage of using non-polarimetric variables is that they allow the algorithm to be applied to a wider variety of radars, not necessarily limited to dual-polarization systems; furthermore, it serves as a backup operational line in case dual-polarization hardware fails or is under maintenance, which is the case for the SOPHY radar.

The proposed algorithm, based on fuzzy logic, uses membership functions to determine the degree of probability of the analyzed fields. The essential part of this method is the definition of its membership functions; these can be easily calculated, adaptable to local environments, or complemented with other radar fields (e.g., dual-polarization) from a small dataset under dry and rainy conditions. Although this study did not delve into the optimization of the weights for each field, these can also be adjusted to improve results; nevertheless, it is clear that the evaluation of the presented method shows a high precision of GC removal using only the Doppler velocity and reflectivity fields.

From the analyzed cases, it is evident that the algorithm presents its main limitations when GC and meteorological echoes occur simultaneously. The stratiform case proves to be the most complex, as the signal intensity and velocity are similar to those of GC; therefore, much of the meteorological signal cannot be recovered or classification errors increase. In contrast, its best performance is found in dry conditions or during convective events. The comparison with the Gabella filter showed limitations in scenarios where the area contaminated with GC is extensive (e.g., 1.0° and 2.6°), highlighting its disadvantage compared to designed and evaluated fuzzy-logic approach. We reaffirm that the Gabella filter should be used as a post-filter in case not all GC echoes could be eliminated.

In general, a significant reduction in the intercept, RMSE, and bias was observed, along with an increase in the correlation between A_{total} and A_{meteo} at different elevations after the application of the filter, this confirms the effectiveness of the implemented SOPHY fuzzy-logic method in filtering GC echoes while preserving the vertical structure of the precipitation system.

The next steps of this work include the optimization of the field weights and the inclusion of polarimetric variables, which are expected to enhance the algorithm's performance as well as radar-based precipitation products

REFERENCES

[1] R. J. Doviak and D. S. Zrnic, *Doppler Radar and Weather Observations*. Academic Press, 1984.

[2] J. C. Hubbert, M. Dixon, and S. M. Ellis, "Weather radar ground clutter. part ii: Real-time identification and filtering," *Journal of Atmospheric and Oceanic Technology*, vol. 26, no. 7, pp. 1181–1197, 2009.

[3] F. Mesnard and H. Sauvageot, "Climatology of anomalous propagation radar echoes in a coastal area," *Journal of Applied Meteorology and Climatology*, vol. 49, no. 11, pp. 2285–2300, 2010.

[4] A. D. Siggia and R. E. Passarelli, "Gaussian model adaptive processing (gmap) for improved ground clutter cancellation and moment calculation," in *Proc. Third European Conf. on Radar Meteorology (ERAD)*, Visby, Suecia, 2004, pp. 67–73.

[5] J. Yin, C. Unal, and H. Russchenberg, "Object-orientated filter design in spectral domain for polarimetric weather radar," *IEEE Transactions on Geoscience and Remote Sensing*, vol. 57, no. 5, pp. 2725–2740, 2019.

[6] D. A. Warde and S. M. Torres, "Staggered-prt sequences for doppler weather radars. part ii: Ground clutter mitigation on the nexrad network using the clean-ap filter," *Journal of Atmospheric and Oceanic Technology*, vol. 34, pp. 703–716, 2017.

[7] S. M. Torres and D. A. Warde, "Ground clutter mitigation for weather radars using the autocorrelation spectral density," *Journal of Atmospheric and Oceanic Technology*, vol. 31, no. 10, pp. 2049–2066, 2014.

[8] J. C. Hubbert, G. Meymaris, U. Romatschke, and M. Dixon, "Using a regression ground clutter filter to improve weather radar signal statistics: Theory and simulations," *Journal of Atmospheric and Oceanic Technology*, vol. 38, pp. 1353–1375, 2021.

[9] M. Steiner and J. Smith, "Use of three-dimensional reflectivity structure for automated detection and removal of nonprecipitating echoes in radar data," *Journal of Atmospheric and Oceanic Technology*, vol. 19, no. 5, pp. 673–686, 2002.

[10] M. Gabella and R. Notarpietro, "Ground clutter characterization and elimination in mountainous terrain," in *Proceedings of ERAD: Use of radar observations in hydrological and NWP models*, 2002, pp. 305–311.

[11] H. Zou, S. Zhang, X. Liang *et al.*, "Improved algorithms for removing isolated non-meteorological echoes and ground clutters in cinrad," *Journal of Meteorological Research*, vol. 32, pp. 584–597, 2018.

[12] S. Moszkowicz, G. J. Ciach, and W. F. Krajewski, "Statistical detection of anomalous propagation in radar reflectivity patterns," *Journal of Atmospheric and Oceanic Technology*, vol. 11, no. 4, pp. 1026–1034, 1994.

[13] J. R. Peter, A. Seed, and P. J. Steinle, "Application of a bayesian classifier of anomalous propagation to single-polarization radar reflectivity data," *Journal of Atmospheric and Oceanic Technology*, vol. 30, no. 9, pp. 1985–2005, 2013.

[14] M. A. Rico-Ramirez and I. D. Cluckie, "Classification of ground clutter and anomalous propagation using dual-polarization weather radar," *IEEE Transactions on Geoscience and Remote Sensing*, vol. 46, no. 7, pp. 1892–1904, 2008.

[15] M. T. Falconi, M. Montopoli, and F. S. Marzano, "Bayesian statistical analysis of ground-clutter for the relative calibration of dual polarization weather radars," *European Journal of Remote Sensing*, vol. 49, no. 1, pp. 933–953, 2016.

[16] H. Lee and S. Kim, "Ensemble classification for anomalous propagation echo detection with clustering-based subset-selection method," *Atmosphere*, vol. 8, no. 1, p. 11, 2017.

[17] M. Grecu and W. F. Krajewski, "An efficient methodology for detection of anomalous propagation echoes in radar reflectivity data using neural networks," *Journal of Atmospheric and Oceanic Technology*, vol. 17, no. 2, pp. 121–129, 2000.

[18] Z. Zhao, H. Wen, L. Wu, R. Li, T. Zhuang, and Y. Zhang, "Non-precipitation echo identification in X-Band dual-polarization weather radar," *Remote Sensing*, vol. 17, no. 17, p. 3023, 2025.

[19] X. Liang and T. Wang, "Ground clutter filter implementation of dual-prf signals for x-band weather radar," in *2018 14th IEEE International Conference on Signal Processing (ICSP)*. IEEE, 2018, pp. 909–914.

[20] D. R. L. Dufton and C. G. Collier, "Fuzzy logic filtering of radar reflectivity to remove non-meteorological echoes using dual polarization radar moments," *Atmospheric Measurement Techniques*, vol. 8, no. 10, pp. 3985–4000, 2015.

[21] S. Das, M. Krishna, Y. Kolte, S. Deshpande, and G. Pandithurai, "Assessment of ground-based x-band radar reflectivity: Attenuation correction and its comparison with space-borne radars over the western ghats, india," *Earth and Space Science*, vol. 7, 2020.

[22] C. Beek, L. H, J. Stricker, R. Uijlenhoet, and H. Russchenberg, "Performance of high-resolution x-band radar for rainfall measurement in the netherlands," *Hydrology and Earth System Sciences Discussions*, vol. 14, 09 2009.

[23] S. Park, V. N. Bringi, V. Chandrasekar, M. Maki, and K. Iwanami, "Correction of radar reflectivity and differential reflectivity for rain attenuation at x band. part i: Theoretical and empirical basis," *Journal of Atmospheric and Oceanic Technology*, vol. 22, no. 11, pp. 1621–1632, 2005.

[24] R. Reinoso-Rondinel, C. Unal, and H. Russchenberg, "Adaptive and high-resolution estimation of specific differential phase for polarimetric x-band weather radars," *Journal of Atmospheric and Oceanic Technology*, vol. 35, no. 3, pp. 555–573, 2018.

[25] G. Buckingham, M. De La Cruz, D. Scipion, J. C. Espinoza, J. Apaza, and G. Kemper, "Implementation of a uav-aided calibration method for a mobile dual-polarization weather radar," *The Egyptian Journal of Remote Sensing and Space Sciences*, vol. 27, pp. 356–368, 2024.

[26] J. C. Espinoza, D. Scipión, A. Valdez, and J. Verástegui, "Sophy: Scanning-system for observations of peruvian hydrometeorological-events," in *2021 IEEE International Conference on Aerospace and Signal Processing (INCAS)*, 2021, pp. 1–4.

[27] J. Apaéstegui, C. Romero, M. Vuille, J. Sulca, and A. Ampuero, "Moisture sources and rainfall δ^{18}o variability over the central andes of peru—a case study from the mantaro river basin," *Water*, vol. 15, no. 10, p. 1867, 2023.

[28] J. L. Flores-Rojas, Y. Silva, L. Suarez-Salas, R. Estevan, J. Valdivia-Prado, M. Saavedra, L. Giraldez, M. Pinas-Laura, D. Scipion, M. Milla, S. Kumar, and D. Martinez-Castro, "Analysis of extreme meteorological events in the central andes of Peru using a set of specialized instruments," *Atmosphere*, vol. 12, no. 3, p. 408, 2021.

[29] M. Heistermann, S. Jacobi, and T. Pfaff, "Technical note: An open source library for processing weather radar data (wradlib)," *Hydrology and Earth System Sciences*, vol. 17, pp. 863–871, 2013.

[30] M. Berenguer, D. Sempere-Torres, C. Corral, and R. Sánchez-Diezma, "A fuzzy logic technique for identifying nonprecipitating echoes in radar scans," *Journal of Atmospheric and Oceanic Technology*, vol. 23, no. 9, pp. 1157–1180, 2006.

[31] T. Mäkinen, J. Ritvanen, S. Pulkkinen, N. Weisshaupt, and J. Koistinen, "Bayesian classification of nonmeteorological targets in polarimetric doppler radar measurements," *Journal of Atmospheric and Oceanic Technology*, vol. 39, no. 10, pp. 1561–1578, 2022.

[32] J. J. Gourley, P. Tabary, and J. Parent du Chatelet, "A fuzzy logic algorithm for the separation of precipitating from nonprecipitating echoes using polarimetric radar observations," *Journal of Atmospheric and Oceanic Technology*, vol. 24, no. 8, pp. 1439–1451, 2007.

[33] X. Hu, J. Ge, J. Du, Q. Li, J. Huang, and Q. Fu, "A robust low-level cloud and clutter discrimination method for ground-based millimeter-wavelength cloud radar," *Atmospheric Measurement Techniques*, vol. 14, no. 2, pp. 1743–1759, 2021.

[34] J. Wang, H. Zou, L. Zhong, and Z. Hu, "Recognition of ground clutter in single-polarization radar based on gated recurrent unit," *Remote Sensing*, vol. 16, no. 23, 2024. [Online]. Available: https://www.mdpi.com/2072-4292/16/23/4609

[35] C. J. Kessinger, S. M. Ellis, J. VanAndel, and J. Yee, "The ap clutter mitigation scheme for the wsr-88d," in *31st International Conference on Radar Meteorology*, Seattle, USA, Aug. 2003.

[36] K. V. Mardia and P. E. Jupp, *Directional statistics*. John Wiley & Sons, 2000.

[37] P. Altube, J. Bech, O. Argemí, T. Rigo, N. Pineda, S. Collis, and J. Helmus, "Correction of dual-prf doppler velocity outliers in the presence of aliasing," *Journal of Atmospheric and Oceanic Technology*, vol. 34, no. 7, pp. 1529–1543, 2017.

[38] V. Tyagi and S. Das, "A probabilistic algorithm for mitigating persistent ground clutter in doppler weather radar," *Journal of Geophysical Research: Atmospheres*, vol. 130, no. 3, p. e2025JD043478, 2025.

[39] W. Nurahman, A. Ali, and R. Fahdiran, "Implementation of gabella method and random forest for ground clutter detection in padang weather radar data," *Spektra: Jurnal Fisika dan Aplikasinya*, vol. 8, no. 3, pp. 167–174, 2023.

[40] M. Gabella, J. Joss, and G. Perona, "Optimizing quantitative precipitation estimates using a noncoherent and a coherent radar operating on the same area," *Journal of Geophysical Research*, vol. 105, no. D2, pp. 2237–2245, 2000.

VI. ACKNOWLEDGMENTS

This work was supported by the Peruvian National Council for Science, Technology and Technological Innovation (CONCYTEC) under Contract PE501087421-2024 PROCIENCIA, "Aplicaciones del radar meteorológico SOPHy para la gestión de riesgo de desastres y recursos hídricos en el Perú: caso El Niño en Piura" (Applications of the SOPHy meteorological radar for disaster risk and water resources management in Peru: El Niño case in Piura).

The AI tool (ChatGPT - OpenAI) was used only for grammar and readability improvements, and all scientific content, analysis, and conclusions were developed and verified by the authors.

CARLOS DEL-CASTILLO VELARDE received the B.S. degree in physics from Universidad Nacional Mayor de San Marcos, Perú in 2019. He is currently a M.S. degree in water resources at Universinal nacional agraria la molina, Lima, Perú. From 2023 to the present he has worked as Research Analyst at Geophysical Institute of Perú. His research interests include remote sensing of the atmosphere, radars, quantitative precipitation estimation, cloud and precipitation physics.

RICARDO REINOSO-RONDINEL Ricardo Reinoso-Rondinel received the B.Sc. degree in electrical engineering from the Pontifical Catholic University of Peru (PUCP), Lima, Peru, in 2006, the M.Sc. degree in electrical and computer engineering from the University of Oklahoma, Norman, OK, USA, in 2011, and the Ph.D. degree from Delft University of Technology (TU Delft), The Netherlands, in 2018. His M.Sc. research was conducted at the Atmospheric Radar Research Center (ARRC), University of Oklahoma, and focused on phased-array weather radar systems, while his doctoral research addressed differential phase processing for dual-polarization weather radars. Following his Ph.D., he conducted postdoctoral research at the Department of Geosciences and Remote Sensing, TU Delft, on Doppler spectral processing of vertically pointing radar systems. In 2019, he joined the University of Bonn, Bonn, Germany, where his research focused on radar-based precipitation nowcasting.

Since 2023, he has been a tenure-track professor at the Department of Civil Engineering, KU Leuven, Leuven, Belgium, in collaboration with the Royal Meteorological Institute of Belgium (KMI). His research interests include dual-polarization weather radar signal processing, quantitative precipitation estimation and nowcasting, multi-sensor data fusion, and data assimilation, with applications in meteorology, hydrology, and high-impact weather monitoring and early warning systems.

DANNY E. SCIPION An electronic engineer from the Pontifical Catholic University of Peru (PUCP), he obtained his Master of Science and PhD in Electrical and Computer Engineering from the University of Oklahoma in 2007 and 2011, respectively. He completed his postdoctoral studies at the École Polytechnique Fédérale de Lausanne (EPFL) in Lausanne, Switzerland, where he collaborated with a mobile dual-polarization X-band radar (MXPol). In 2013, he returned to the Geophysical Institute of Peru (IGP) as a research scientist at the Jicamarca Radio Observatory. Between 2018 and 2020, he served as the IGP's scientific director. Since September 2021, he has been the director of the Jicamarca Radio Observatory. In April 2025, following the approval of the law strengthening the IGP (Geophysical Institute of Peru), he became the Director of Geospace Sciences, where he continues his research activities. His most recent research focuses on the analysis of data from the SOPHy meteorological radar constructed by the IGP, as well as studies of the effects of magnetic storms on Peru and the climatology of mesospheric echoes acquired with the Jicamarca ionospheric radar.

JAIRO M. VALDIVIA-PRADO Jairo M. Valdivia-Prado received the B.Sc. degree and the Engineer degree in environmental engineering from Universidad Nacional José Faustino Sánchez Carrión, Lima, Perú, in 2015 and 2018, respectively, and the M.S. degree in atmospheric and oceanic sciences from the University of Colorado, Boulder, CO, USA, in 2025. He is currently a Ph.D. candidate in atmospheric and oceanic sciences with the University of Colorado, Boulder. From 2016 to 2023, he was with the Geophysical Institute of Peru, Lima, serving as a Research Assistant, where he focused on signal processing for cloud profilers and quantitative precipitation estimation. Since 2023, he has been a Research Assistant with the University of Colorado. His current research is focused on radar signal processing, cloud microphysics, precipitation studies, and multi-frequency radar retrievals for particle type identification

DANIEL MARTÍNEZ CASTRO received the B.S. degree in physics from Universidad de La Habana, Cuba in 1976 and the PhD in physics at Academia de Ciencias de Cuba in 1996. From 1976 to 1981 he worked as assistant trainer in two universities and from 1982 to 2017 he worked as researcher and Head of the Center for Atmospheric Physics in the Cuban Institute of Meteorology. From 2017 to the present he has worked in different periods as researcher and vice-director in the Peruvian Geophysical institute and in the Peruvian National Research Institute on Glaciers and Mountain Ecosystems. His present research interest includes climate change, Amazon drought, cloud and precipitation physics and dynamics in mountain environment and the use of radars in qualitative precipitation estimation. Dr. Martínez-Castro has been senior Associate of the International Centre for Theoretical Physics and lead author of the IPCC Sixth Report, Group I.

YAMINA SILVA-VIDAL received the Meteorological Engineer Class I degree in 1992, the M.S. degree in Engineering in 1992, and the Ph.D. degree with a specialization in Physical-Mathematical Sciences in 1996, all from the State Hydrometeorological Institute of Russia. Since 1998, she has been with the Geophysical Institute of Peru, where she is currently a Principal Scientific Researcher. Her research interests include atmospheric physics, with a focus on understanding the physical processes associated with extreme events in the Peruvian Andes. She has led several research projects aimed at strengthening this field, including the implementation of the Atmospheric Physics and Microphysics Laboratory (LAMAR), located at 3300 m above sea level. She has also promoted the development of meteorological radar systems, including the SOPHy radar.